

Article

Response of Population Canopy Color Gradation Skewed Distribution Parameters of the RGB Model to Micrometeorology Environment in *Begonia Fimbristipula Hance*

Pei Zhang ¹, Zhengmeng Chen ², Fuzheng Wang ³, Rong Wang ⁴, Tingting Bao ¹, Xiaoping Xie ¹, Ziyue An ⁵, Xinxin Jian ² and Chunwei Liu ^{6,*} 

- ¹ Jiangsu Meteorological Bureau, Nanjing 210008, China; qhzx_zp@foxmail.com (P.Z.); 13813399860@qq.com (T.B.); qhzx_xx@foxmail.com (X.X.)
- ² Longyan Company of Fujian Provincial Tobacco Corporation, Longyan 364000, China; rei_shadow@126.com (Z.C.); ydjianxx@163.com (X.J.)
- ³ QinGengRen Modern Agricultural Science and Technology Development (Huai'an) Co., Ltd., Huai'an 223001, China; fzhwang@sina.cn
- ⁴ Jiangsu Key Laboratory for the Research and Utilization of Plant Resources, Institute of Botany, Jiangsu Province and Chinese Academy of Sciences, Nanjing 210014, China; njau2010216002@163.com
- ⁵ Department of Chemistry, Faculty of Science, Carleton University, Ottawa, ON K1S 5B6, Canada; ziyuean@cmail.carleton.ca
- ⁶ Jiangsu Provincial Key Laboratory of Agricultural Meteorology, College of Applied Meteorology, Nanjing University of Information Science and Technology, Nanjing 210044, China
- * Correspondence: liucw@nuist.edu.cn



Citation: Zhang, P.; Chen, Z.; Wang, F.; Wang, R.; Bao, T.; Xie, X.; An, Z.; Jian, X.; Liu, C. Response of Population Canopy Color Gradation Skewed Distribution Parameters of the RGB Model to Micrometeorology Environment in *Begonia Fimbristipula Hance*. *Atmosphere* **2022**, *13*, 890.

<https://doi.org/10.3390/atmos13060890>

Academic Editors: Demetrios E. Tssemelis, Nikolaos Skondras and Nikolaos Proutsos

Received: 26 April 2022

Accepted: 19 May 2022

Published: 30 May 2022

Publisher's Note: MDPI stays neutral with regard to jurisdictional claims in published maps and institutional affiliations.



Copyright: © 2022 by the authors. Licensee MDPI, Basel, Switzerland. This article is an open access article distributed under the terms and conditions of the Creative Commons Attribution (CC BY) license (<https://creativecommons.org/licenses/by/4.0/>).

Abstract: The high quality and efficient production of greenhouse vegetation depend on micrometeorology environmental adjusting such as system warming and illumination supplement. In order to improve the quantity, quality, and efficiency of greenhouse vegetation, it is necessary to figure out the relationship between the crop growth conditions and environmental meteorological factors, which could give constructive suggestions for precise control of the greenhouse environment and reduce the running costs. The parameters from the color information of the plant canopy reflect the internal physiological conditions, thus, the RGB model has been widely used in the color analysis of digital pictures of leaves. We take photographs of *Begonia Fimbristipula Hance* (BFH) growing in the greenhouse at a fixed time every day and measure the meteorological factors. The results showed that the color scale for the single leaf, single plant, and the populated canopy of the BFH photographs all have skewed cumulative distribution histograms. The color gradation skewness-distribution (CGSD) parameters of the RGB model were increased from 4 to 20 after the skewness analysis, which greatly expanded the canopy leaf color information and could simultaneously describe the depth and distribution characteristics of the canopy color. The 20 CGSD parameters were sensitive to the micrometeorology factors, especially to the radiation and temperature accumulation. The multiple regression models of mean, median, mode, and kurtosis parameters to microclimate factors were established, and the spatial models of skewness parameters were optimized. The models can well explain the response of canopy color to microclimate factors and can be used to monitor the variation of plant canopy color under different micrometeorology.

Keywords: RGB model; skewed distribution; population canopy color gradation; microclimate environment; response

1. Introduction

Meteorological conditions are crucial factors that determine crop growth and leaf development [1,2]. Facility agriculture is an efficient crop production through the precise regulating of microclimate within the greenhouse [3–5]. Clarifying the relationships between plant physiological and ecological indicators and meteorological conditions are

the basic method for quantitative assessment of agro-meteorological conditions, assessing the agro-meteorological disaster losses, predicting the yield, and applying the intelligent micrometeorology control of agricultural production. Thus, it is the right path to find the determining parameters that have a close relationship with meteorological factors and reflect plant growth status sensitively.

Digital image technology is well-developed and high-resolution camera equipment is widely used, with digital imaging technology having the obvious advantages of high resolution and low cost in the research of plant phenotypes [6,7]. A digital color image is not only convenient to obtain [8], but also contains abundant information about plant morphology, structure, and color gradation [9–11], which can reflect the internal status of plants. The RGB color model is the popularly used color representation for digital images [12]. The parameters of the traditional RGB model are mainly the mean values of each color channel and their combined values, which can approximately describe the color depth of the leaves and estimate the chlorophyll content of the leaves [13–18]. Moreover, the RGB model reflects the soil moisture and nutrient levels [19–22]. However, the mean values of image parameters are not comprehensive enough in the description of color distribution [23], as a result, the RGB model is generally used in the studies of water, fertility, and disease which may drastically change the leaf color [8,24–26]. The RGB model is also an effective method to reflect the relationship between the image information and the variation of environmental factors.

The quantitative analysis of mega-high quality digital photographs could explain the genotype-by-environment interactions in plant phenotypes [27]. The variation of meteorological factors affects the physiological and biochemical characters of plants slightly, such as influencing the openness of the stomata [28], changing the arrangement of the chloroplast [29], and increasing or decreasing the photosynthesis rate of the leaves [30,31]. All these affections change the plant's color under a visible spectrum [32]. Therefore, the image color information parameters are used as representative references to reflect the meteorological environment of the growing plant. Skewed analysis expanded the RGB model parameters from the mean to the mean, median, mode, skewness, and kurtosis, with the number of parameters from 4 to 20 [33]. The color gradation skewness-distribution (CGSD) parameters describe leaf color information more accurately and comprehensively than the traditional mean parameters [33], including whether the color gradation distribution of a single plant varies the same as the leaf, and the field scale determines its sensitivity in response to the environmental meteorological factors. The CGSD for all scales varying consistently helps to construct an effective model between the external meteorological factors and morphological parameters of the plant. The quantitative evaluation of agro-meteorological conditions for a plant can be achieved by combining canopy color information indexes corresponding to different morphological parameters of plants, to provide information that supports precise management of plant production.

Begonia Fimbristipula Hance (BFH) is a vegetation type widely used for medicine and food. BFH has abundant anthocyanins, polyphenols, and flavonoids and a strong antioxidant capacity [34–36]. BFH is cultivated in facilities that have a warm and humid environment to ensure annual cultivation [37]. After planting BFH in a glass greenhouse and collecting the meteorological factors and canopy photographs, the relationship between changes in canopy color and the meteorological factors in the facility environment was analyzed. The purpose of this research is: (1) to quantify the mathematical relationship between CGSD parameters and meteorological factors, and increase the accuracy of quantifying the changes in population canopy color with meteorological changes; (2) to construct population canopy color–meteorological response models by using the relationship of CGSD parameters and meteorological factors, including temperature, humidity, and solar radiation, and; (3) to provide new methods from the RGB model to monitor the patterns of canopy color variations due to meteorological environment changes. The results may construct the crop growth model based on the CGSD parameters of the RGB model, and provide a new approach for intelligent control of facility agricultural production.

2. Materials and Methods

2.1. Plant Material and Growth Conditions

The glass greenhouse for the experiment is in Guli Modern Agriculture Demonstration Park, Jiangning District, Nanjing, Jiangsu, China (24°57' N, 116°30' E). The BFH were potted by the rooting of cuttings and planted with a total nutrient matrix which was in the proportion of N: P₂O₅: K₂O in a 100 g matrix at 20:10:20, trace elements included Cu, Fe, Zn, Mn, B, and Mo ≥ 1%, and pH 5.85. Moreover, the matrix contained an active accelerator and sustained release agent of poly-fertilizer. The BFH experiment had 2 replicates, and each replicate contained 24 potted plants. The first growing period of BFH was from 1 December 2018 to 17 February 2019, and after cutting off the 10 cm top length on 18 February, BFH continued growing in the second growth period from 19 February 2019 to 11 April 2019.

2.2. Meteorological Data Acquisition

Meteorological data were obtained from the agricultural meteorological observation station (DZZ4, Jiangsu Provincial Radio Science Research Institute Co., LTD., Wuxi, China) in the facility. The observed meteorological elements included daily meteorological elements, such as the daily mean temperature (T_{dm}), daily mean relative humidity (RH_{dm}), daily mean ground temperature (TG_{dm}), daily mean soil temperature at 10 cm (TS_{dm-10c}), daily mean vapor pressure (VP_{dm}), daily mean dew point temperature (TD_{dm}), daily total global radiation (GR_{dt}), and daily total photosynthetically active radiation (PAR_{dt}). The accumulated temperature (AT), accumulated global radiation (AGR), and accumulated photosynthetically active radiation (APAR) were calculated from T_{dm} , GR_{dt} , and PAR_{dt} .

$$AT = \sum T_{dm} \quad (1)$$

$$AGR = \sum GR_{dt} \quad (2)$$

$$APAR = \sum PAR_{dt} \quad (3)$$

2.3. Canopy Image Collection

Canopy color images of BFH were collected in the facility by a monitoring camera (DH-SD-65F630U-HN-Q, Zhejiang Dahua Technology Co., Ltd., Hangzhou, China) with an image resolution of 1920 × 1080, and the installation height was 280 cm (Figure 1). The camera with a vertical lens was set with a fixed focal length shooting and automatic white balance and adopted a fixed time shooting mode to take a photograph at set times of 9:03 a.m. every day. The 117 images from 3 groups without direct sunlight were selected for analysis, including 102 images in the first growth period (1 December 2018 to 17 February 2019) of 2 replicates with 51 pictures each, and 15 images in the second growth period (19 February 2019 to 11 April 2019).

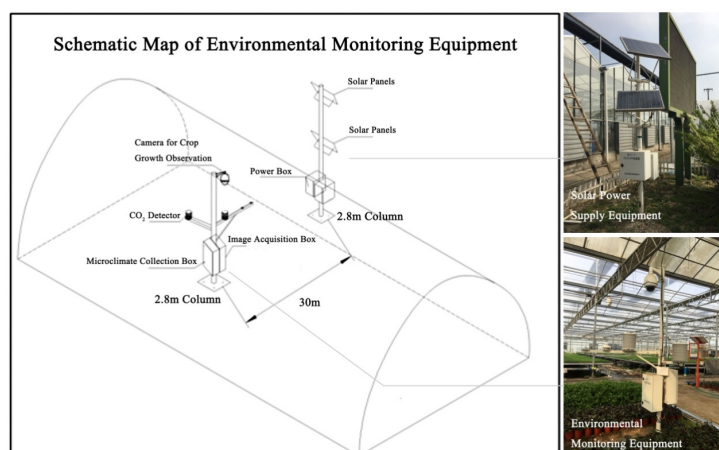


Figure 1. Schematic map of microclimate observation and digital camera in the glass greenhouse.

2.4. Cutting and Denoising of the Image

Adobe Photoshop V8.0 software (San Jose, CA, USA) and MATLAB2016R software (referred to as MATLAB [Math Works, Natick, MA, USA]) were primarily used to cut and denoise the BFH original image [38,39] (Figure 2a).

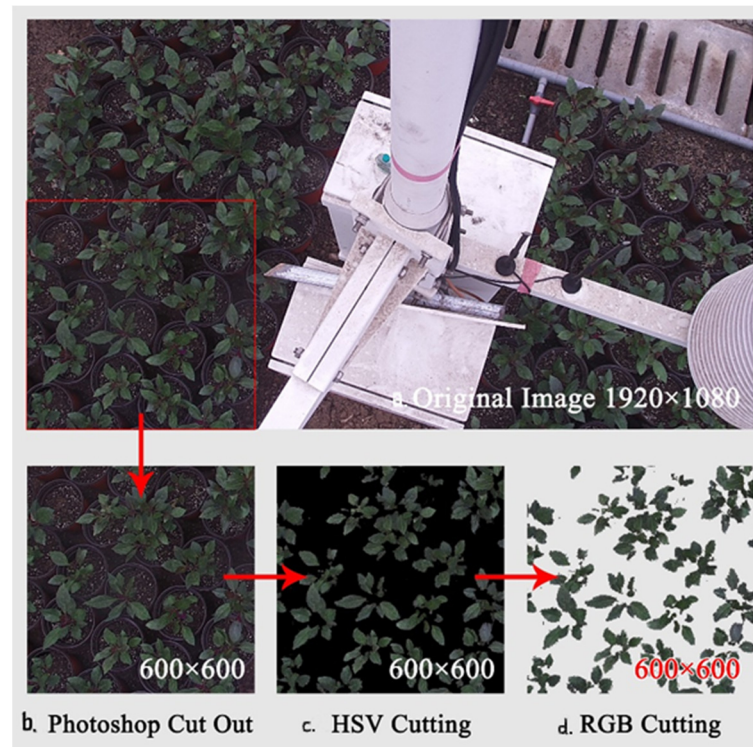


Figure 2. Flow map of Cutting and Denoising of the Image.

1. Adobe Photoshop CS software (San Jose, CA, USA) was primarily used to intercept the range of 600×600 in the lower-left corner of the image, and the processed image was saved in a JPG image format (Figure 2b).
2. The *rgb2hsv* function of MATLAB was used to convert RGB images into HSV images. Double cycle operation was used to set the H-value of the image background to 0 (i.e., black), while the H value of the plant remains unchanged. The *hsv2rgb* function was used to convert the processed HSV image into an RGB image (Figure 2c).
3. The double cycle operation of MATLAB was used again to filter the color threshold value of the image processed in the previous step. The color opacity of the black part of the image was adjusted to 0 (that is, completely transparent), and the color image of the target leaf or canopy with the transparent background was saved as a PNG image mode (Figure 2d).

2.5. Information Collection of the RGB Image

Transformation of double-precision arrays of the image. MATLAB was used to extract and analyze BFH RGB images. After reading color images by using the *imread* function, *image(:, :, 1)*, *image(:, :, 2)*, *image(:, :, 3)*, and the *rgb2gray* function were respectively used to read every pixel gradation of red, green and blue channels, as well as gray-level images. The full circulation algorithm was used to retrieve and record the non-black pixel index codes of these pixels, which were combined with an array of leaf color gradation. Then the *double* function was used to transform it into double precision arrays again.

Establishment of the canopy color gradation skewness-distribution (CGSD) parameters table. The *mean*, *median*, *mode*, *std*, *skewness* and *kurtosis* functions were used to acquire the mean, median, mode, standard Deviation, skewness, and kurtosis of the double-precision arrays of red, green, and blue channels, as well as gray-level images [33].

The CGSD parameters were obtained, including R_{Mean} , R_{Median} , R_{Mode} , $R_{Skewness}$, $R_{Kurtosis}$, G_{Mean} , G_{Median} , G_{Mode} , $G_{Skewness}$, $G_{Kurtosis}$, B_{Mean} , B_{Median} , B_{Mode} , $B_{Skewness}$, $B_{Kurtosis}$, Y_{Mean} , Y_{Median} , Y_{Mode} , $Y_{Skewness}$, and $Y_{Kurtosis}$ (Table 1). Finally, the CGSD parameters tables of color gradation distribution of BFH RGB images were formed.

Table 1. Color gradation skewness–distribution (CGSD) parameters.

Channel	CGSD Parameters				
	Mean	Median	Mode	Skewness	Kurtosis
Red Channel (R)	R_{Mean}	R_{Median}	R_{Mode}	$R_{Skewness}$	$R_{Kurtosis}$
Green Channel (G)	G_{Mean}	G_{Median}	G_{Mode}	$G_{Skewness}$	$G_{Kurtosis}$
Blue Channel (B)	B_{Mean}	B_{Median}	B_{Mode}	$B_{Skewness}$	$B_{Kurtosis}$
Gray Image (Y)	Y_{Mean}	Y_{Median}	Y_{Mode}	$Y_{Skewness}$	$Y_{Kurtosis}$

Array distribution normality testing. The *lillietest* and *jbtest* functions were used to conduct the Lilliefors and Jarque-Bera tests of normal distribution for the color gradation distribution of red, green, and blue channels, as well as gray-level images of BFH RGB images.

2.6. Prediction Model Construction and Goodness-of-Fit Detection

Correlation Analysis of 20 CGSD Parameters to Microclimate Factors. The Cor package of R was used to analyze the relationship between 20 CGSD parameters of population canopy in RGB images of BFH and the corresponding microclimate factors, including daily meteorological factors (T_{dm} , RH_{dm} , TG_{dm} , TS_{dm-10c} , VP_{dm} , TD_{dm} , GR_{dt} , and PAR_{dt}) and photothermal accumulation factors (AT, AGR, and APAR), which were collected for significant examination with a double tail inspection.

Linear prediction models establishment. By using R, the linear prediction models (Y1–Y20) of 20 CGSD parameters of population canopy in RGB images of BFH were established by a regression approach based on the *least-square* method, with meteorological factors as the independent variables. The probability of F-to-enter of the models was set to 0.050 or less, while the probability of F-to-remove was set to 0.100 or more. Decision coefficient optimization, significance test of regression model and regression coefficient, and collinearity diagnosis of independent variables of the regression model were conducted for the alternative regression models in turn [40], and the optimal regression models were finally determined.

Spatial polynomial model establishment. Two photothermal accumulation factors with the correlation coefficient of highest absolute value with CGSD parameters were selected as the independent variable, and the spatial polynomial models (Z1–Z4) of skewness of red, green, and blue channels, as well as gray-level images, were established by using polynomial fitting in the Curve Fitting Tool of R.

3. Results

3.1. Skew Analysis of the Distribution of Leaf Color Gradation of the RGB Images

After analyzing the cumulative distribution of color gradation of the 117 selected images of BFH, we found that all the red, green, and blue channels, and the gray-level for single leaf, single plant, and population canopy images showed a left-skewed distribution (Figure 3). Lilliefors and Jarque-Bera normality tests also indicated that color gradation data did not distribute normally (Supplementary Table S1). Twenty color gradient skewness–distribution (CGSD) parameters were obtained including the mean, median, mode, skewness, and kurtosis for the red, green, and blue channels, as well as the gray-level image, for each canopy image, respectively. These parameters can describe not only the depth of canopy color but also its distribution.

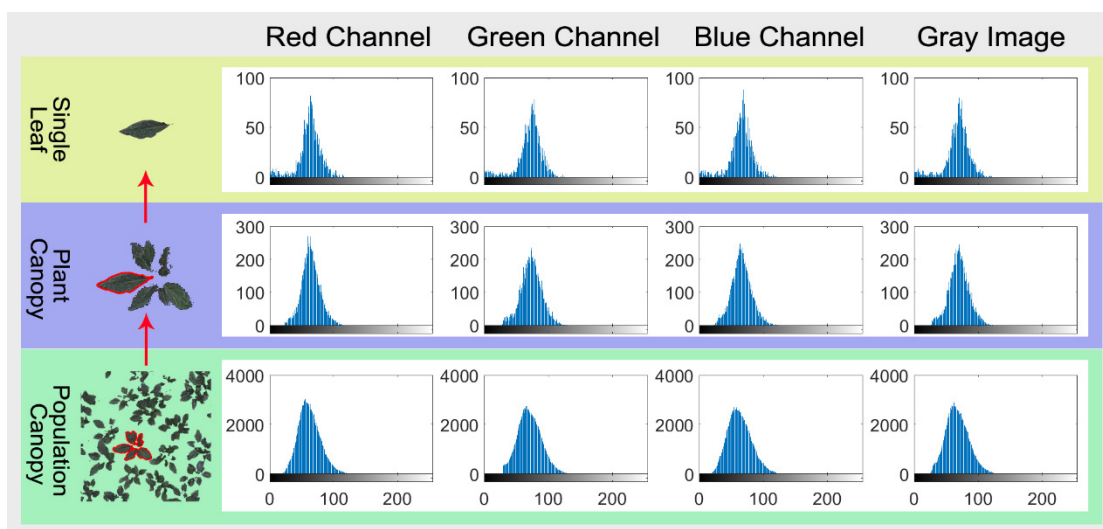


Figure 3. RGB model color gradation distribution of single leaf, plant canopy, and population canopy images of *Begonia Fimbristipula Hance* (BFH). The cumulative frequency histogram of red, green, and blue channels, as well as gray-level images, were drawn using the *imhist* function of MATLAB. The X-axis is the color gradation value, and the Y-axis is the cumulative frequency.

The main distribution of color gradation is positive skewness for RGB channels and the gray-level image near the value of 0. This increment of positive skewness as the canopy develops reflected the leaf color transit from light green to dark green (Figure 4).

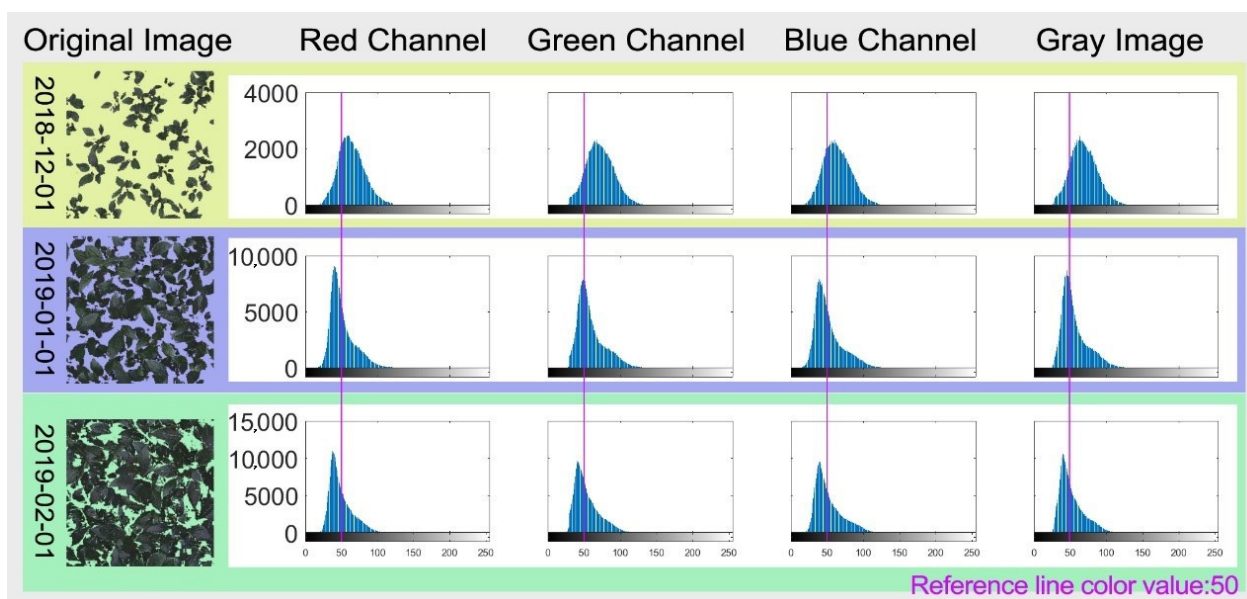


Figure 4. RGB model color gradation distribution of population canopy images of BFH on 3 different dates. The cumulative frequency histogram of red, green, and blue channels, as well as gray-level images, were drawn using the *imhist* function of MATLAB. The X-axis is the color gradation value, and the Y-axis is the cumulative frequency.

3.2. Correlation Analysis Microclimate Factors in Glasshouse and Population Canopy CGSD Parameters

The relationship between 20 CGSD parameters and the microclimate factors including daily meteorological factors (T_{dm} , RH_{dm} , TG_{dm} , TS_{dm-10c} , VP_{dm} , TD_{dm} , GR_{dt} , and PAR_{dt}) and accumulative factors (AT, AGR, and APAR) are shown in Table 2. Table 2 indicates that temperature, humidity, ground temperature, soil temperature at 10 cm, and solar radiation

were significantly correlated with the CGSD parameters. The accumulated temperature and solar radiation (AT, AGR, and APAR) had an extremely significant correlation with the 20 CGSD parameters, with the correlation coefficients higher than 0.8. The parameters of mean, median, and mode, which represented color depth, showed a significant positive correlation with the meteorological factors, while the parameters of skewness and kurtosis representing color uniformity showed an obviously negative correlation.

Table 2. Spearman correlation coefficient of population canopy CGSD parameters of BFH and microclimate factors.

	T _{dm}	RH _{dm}	TG _{dm}	TS _{dm-10c}	VP _{dm}	TD _{dm}	GR _{dt}	PAR _{dt}	AT	AGR	APAR
R _{Mean}	-0.249	0.606 **	0.278 *	0.629 **	-0.025	-0.029	-0.24	-0.251	-0.865 **	-0.856 **	-0.860 **
R _{Median}	-0.253	0.605 **	0.280 *	0.641 **	-0.024	-0.033	-0.227	-0.235	-0.843 **	-0.836 **	-0.840 **
R _{Mode}	-0.257	0.584 **	0.315 *	0.690 **	-0.041	-0.045	-0.247	-0.251	-0.815 **	-0.813 **	-0.816 **
R _{Skewness}	0.225	-0.586 **	-0.292 *	-0.641 **	0.003	0.01	0.214	0.224	0.853 **	0.846 **	0.850 **
R _{Kurtosis}	0.142	-0.503 **	-0.265	-0.519 **	-0.054	-0.047	0.113	0.131	0.792 **	0.774 **	0.779 **
G _{Mean}	-0.282 *	0.633 **	0.236	0.588 **	-0.067	-0.053	-0.344 *	-0.358 **	-0.950 **	-0.947 **	-0.949 **
G _{Median}	-0.289 *	0.641 **	0.246	0.613 **	-0.068	-0.057	-0.343 *	-0.355 *	-0.931 **	-0.929 **	-0.931 **
G _{Mode}	-0.295 *	0.607 **	0.25	0.623 **	-0.088	-0.079	-0.326 *	-0.334 *	-0.901 **	-0.901 **	-0.902 **
G _{Skewness}	0.231	-0.598 **	-0.307 *	-0.668 **	0.008	0.01	0.257	0.268	0.866 **	0.864 **	0.867 **
G _{Kurtosis}	0.157	-0.507 **	-0.261	-0.526 **	-0.031	-0.033	0.176	0.197	0.855 **	0.844 **	0.848 **
B _{Mean}	-0.332 *	0.625 **	0.235	0.632 **	-0.105	-0.112	-0.284 *	-0.293 *	-0.794 **	-0.789 **	-0.793 **
B _{Median}	-0.317 *	0.619 **	0.252	0.654 **	-0.088	-0.097	-0.272	-0.278 *	-0.790 **	-0.787 **	-0.790 **
B _{Mode}	-0.263	0.577 **	0.321 *	0.716 **	-0.047	-0.054	-0.292 *	-0.298 *	-0.750 **	-0.751 **	-0.754 **
B _{Skewness}	0.243	-0.588 **	-0.294 *	-0.656 **	0.023	0.028	0.242	0.252	0.864 **	0.860 **	0.863 **
B _{Kurtosis}	0.205	-0.517 **	-0.238	-0.527 **	0.012	0.017	0.164	0.181	0.821 **	0.808 **	0.812 **
Y _{Mean}	-0.281 *	0.632 **	0.25	0.610 **	-0.06	-0.053	-0.313 *	-0.327 *	-0.922 **	-0.917 **	-0.920 **
Y _{Median}	-0.283 *	0.630 **	0.258	0.630 **	-0.059	-0.056	-0.304 *	-0.314 *	-0.899 **	-0.896 **	-0.898 **
Y _{Mode}	-0.271	0.608 **	0.285 *	0.665 **	-0.056	-0.051	-0.316 *	-0.323 *	-0.884 **	-0.884 **	-0.884 **
Y _{Skewness}	0.229	-0.593 **	-0.305 *	-0.661 **	0.005	0.01	0.239	0.25	0.858 **	0.854 **	0.857 **
Y _{Kurtosis}	0.159	-0.508 **	-0.259	-0.524 **	-0.033	-0.031	0.154	0.173	0.832 **	0.818 **	0.822 **

Note: A Spearman correlation analysis of SPSS software was used on 20 CGSD parameters (R_{Mean}, R_{Median}, R_{Mode}, R_{Skewness}, R_{Kurtosis}, G_{Mean}, G_{Median}, G_{Mode}, G_{Skewness}, G_{Kurtosis}, B_{Mean}, B_{Median}, B_{Mode}, B_{Skewness}, B_{Kurtosis}, Y_{Mean}, Y_{Median}, Y_{Mode}, Y_{Skewness}, and Y_{Kurtosis}) and the microclimate factors including daily meteorological factors (T_{dm}, RH_{dm}, TG_{dm}, TS_{dm-10c}, VP_{dm}, TD_{dm}, GR_{dt}, and PAR_{dt}) and photothermal accumulation factors (AT, AGR, and APAR) (n = 51). ** indicates significant correlation according to a two-tailed test (p < 0.01), * indicates significant correlation according to a two-tailed test (p < 0.05), the same as below.

3.3. Multiple Linear Relationships of the Microclimate Factors and Population Canopy CGSD Parameters

Multiple linear relationships between population canopy CGSD parameters and microclimate factors were established by the stepwise regression method using the ordinary least square method (OLS) (Table 3). Table 3 showed that all the multivariate determination coefficients (R²) of the population canopy color-meteorological response models equation were greater than 0.7, indicating that the equation well explained the response of BFH population canopy CGSD parameters to microclimate factors. The R² of the red and green channels, as well as the gray-level image, was 0.692–0.954, which was better than those of the blue channel with 0.674–0.791. The model between the mean of green channel and accumulated temperature, daily mean relative humidity, and the daily total photosynthetically active radiation had the highest R² of 0.954. Moreover, all the models were significant (p < 0.01).

All the models were verified by between-group and outside-group samples (Table 4 and Figures 5–7), which indicated that the population canopy color fitting models performed well in predicting the mean, median, mode, and kurtosis. The accuracy of prediction of the skewness was about 80%, while other CGSD parameters exceeded 90%, with the mean of the blue channel, as well as the gray-level image exceeding 95% (Table 4) in the same modeling group samples. Similarly, the accuracy of prediction of the mean, median, and mode of RGB channels and the gray-level image was 90%, the kurtosis was about 75%, and the skewness was 53–58% in the between-group prediction. The accuracy of prediction of other CGSD parameters was 80% with the exception of the skewness and kurtosis of the red channel, the mode, and skewness of the green channel, and the median of the gray-level image in the outside-group. Moreover, the accuracy of prediction of the kurtosis of the green and blue channels, and the gray-level image exceeded 85%.

Table 3. Population canopy color-meteorological response models of BFH and their goodness of fit.

Model	R-Square	Adjusted R-Square	RMSE	F Value	Significance F	
R _{Mean}	Y1 = 11.556 - 0.017x ₁ + 0.524x ₂ + 0.549x ₃	0.848	0.839	2.456	87.634	0.000
R _{Median}	Y2 = - 28.395 - 0.015x ₁ + 0.629x ₂ + 0.703x ₃ + 1.871x ₄	0.868	0.857	2.630	75.860	0.000
R _{Mode}	Y3 = 14.284 - 0.024x ₅ + 2.596x ₄	0.746	0.735	3.668	70.458	0.000
R _{Skewness}	Y4 = 2.100 + 0.001x ₁ - 0.199x ₄ + 0.107x ₆	0.803	0.791	0.142	63.968	0.000
R _{Kurtosis}	Y5 = 5.371 - 0.010 x ₁ - 0.024x ₇ - 0.028 x ₂	0.706	0.688	0.382	37.703	0.000
G _{Mean}	Y6 = 27.424 - 0.022x ₁ + 0.464x ₂ + 0.349x ₃	0.954	0.951	1.609	327.337	0.000
G _{Median}	Y7 = 34.402 - 0.036x ₅ + 0.366 x ₂	0.906	0.902	2.548	230.359	0.000
G _{Mode}	Y8 = 30.294 - 0.037x ₅ + 0.342 x ₂	0.845	0.839	3.456	130.821	0.000
G _{Skewness}	Y9 = 1.501 + 0.030x ₅ - 0.052x ₇ - 0.013 x ₂	0.831	0.820	0.138	76.900	0.000
G _{Kurtosis}	Y10 = 2.824 + 0.002x ₁	0.732	0.726	0.310	133.539	0.000
B _{Mean}	Y11 = 30.430 - 0.013x ₁ + 0.341x ₂	0.703	0.691	3.136	56.787	0.000
B _{Median}	Y12 = -6.307 - 0.012x ₁ + 0.380x ₂ + 2.094 x ₄	0.752	0.736	3.470	47.483	0.000
B _{Mode}	Y13 = 4.464 - 0.020 x ₅ + 3.267x ₄	0.695	0.683	4.028	54.781	0.000
B _{Skewness}	Y14 = 1.716 + 0.001x ₁ - 0.083x ₄	0.791	0.782	0.145	90.164	0.000
B _{Kurtosis}	Y15 = 2.874 + 0.002x ₁	0.674	0.668	0.346	101.377	0.000
Y _{Mean}	Y16 = 38.927 - 0.019x ₁ + 0.307x ₂	0.892	0.888	2.240	198.372	0.000
Y _{Median}	Y17 = 30.819 - 0.021x ₁ + 0.368x ₂	0.855	0.848	2.956	140.973	0.000
Y _{Mode}	Y18 = 26.665 - 0.032 x ₅ + 2.144 x ₄	0.825	0.818	3.440	113.213	0.000
Y _{Skewness}	Y19 = 1.818 + 0.001x ₁ - 0.092 x ₄	0.784	0.775	0.156	87.302	0.000
Y _{Kurtosis}	Y20 = 2.901 + 0.002x ₁	0.692	0.686	0.355	110.029	0.000

Note: x₁ is the accumulated temperature, x₂ is the daily mean relative humidity, x₃ is the daily total photosynthetically active radiation, x₄ is the daily mean soil temperature at 10 cm, x₅ is the accumulated photosynthetically active radiation, x₆ is the daily minimum ground temperature, x₇ is the accumulated global radiation.

Table 4. Analytical results of prediction accuracy of population canopy color-meteorological response models.

Model	Prediction Sample Data	Modeling Group			Between-Group Prediction			Outside-Group Prediction			Average
		Eliminate Abnormal Data	Predictive Accuracy	Prediction Sample Data	Eliminate Abnormal Data	Predictive Accuracy	Prediction Sample Data	Eliminate Abnormal Data	Predictive Accuracy		
R _{Mean}	Y1	51	0	96.27%	51	0	92.89%	15	0	90.92%	94.11%
R _{Median}	Y2	51	0	96.02%	51	0	91.98%	15	0	84.90%	92.84%
R _{Mode}	Y3	51	0	92.89%	51	0	92.47%	15	0	87.87%	92.06%
R _{Skewness}	Y4	51	0	80.98%	51	10	53.21%	15	3	70.30%	68.80%
R _{Kurtosis}	Y5	51	0	90.48%	51	0	72.53%	15	0	73.56%	80.49%
G _{Mean}	Y6	51	0	97.98%	51	0	93.55%	15	0	93.71%	95.50%
G _{Median}	Y7	51	0	96.29%	51	0	91.97%	15	0	80.08%	92.33%
G _{Mode}	Y8	51	0	94.14%	51	0	92.38%	15	0	77.33%	91.22%
G _{Skewness}	Y9	51	1	76.29%	51	9	52.40%	15	7	35.12%	63.73%
G _{Kurtosis}	Y10	51	0	92.98%	51	0	76.64%	15	0	86.75%	85.06%
B _{Mean}	Y11	51	0	95.46%	51	0	92.05%	15	0	84.66%	92.59%
B _{Median}	Y12	51	0	94.53%	51	0	90.57%	15	0	85.42%	91.64%
B _{Mode}	Y13	51	0	92.66%	51	0	92.65%	15	0	84.46%	91.60%
B _{Skewness}	Y14	51	1	82.21%	51	8	56.11%	15	3	82.39%	72.36%
B _{Kurtosis}	Y15	51	0	92.17%	51	0	74.21%	15	0	84.12%	83.31%
Y _{Mean}	Y16	51	0	96.95%	51	0	93.33%	15	0	89.60%	94.43%
Y _{Median}	Y17	51	0	90.26%	51	0	93.64%	15	0	67.68%	88.84%
Y _{Mode}	Y18	51	0	94.11%	51	0	93.15%	15	0	87.27%	92.82%
Y _{Skewness}	Y19	51	2	80.43%	51	10	58.03%	15	3	84.64%	73.81%
Y _{Kurtosis}	Y20	51	0	92.56%	51	0	76.04%	15	0	86.53%	84.59%

Note: Predictive accuracy = (1 - |predictive value-measured value| / measured) × 100%.

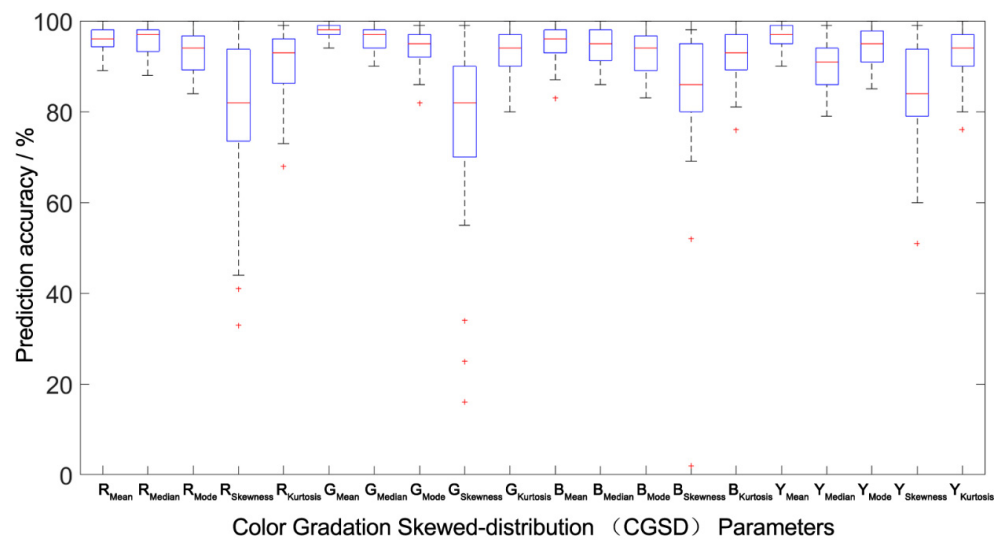


Figure 5. Prediction accuracy interval analysis of the population canopy color-meteorological response models of the modeling group. The *Boxplot* function of MATLAB was used to draw the accuracy percentile distribution diagram of the population canopy CGSD parameters prediction model. The blue box in the figure represents the prediction accuracy of the model distributed between

25% and 75%. The shorter the box, the better the degree of data concentration. The red line in the box represents the median distribution of prediction accuracy, and the dotted line at both ends outside the box represents the endpoint value (maximum and minimum) of the prediction data distribution. The shorter the distance between the two endpoint values, the better the degree of data concentration. The red cross outside the box represents abnormal data. The fewer abnormal data, the better the degree of data distribution concentration.

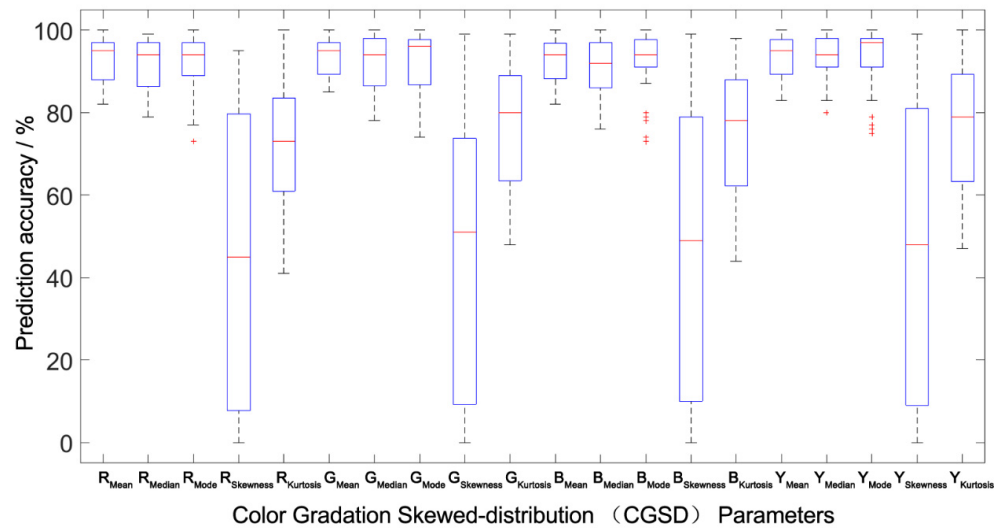


Figure 6. Prediction accuracy interval analysis of the population canopy color-meteorological response models of the between-group. The *Boxplot* function of MATLAB was used to draw the accuracy percentile distribution diagram of the population canopy CGSD parameters prediction model. The blue box in the figure represents the prediction accuracy of the model distributed between 25% and 75%. The shorter the box, the better the degree of data concentration. The red line in the box represents the median distribution of prediction accuracy, and the dotted line at both ends outside the box represents the endpoint value (maximum and minimum) of the prediction data distribution. The shorter the distance between the two endpoint values, the better the degree of data concentration. The red cross outside the box represents abnormal data. The fewer abnormal data, the better the degree of data distribution concentration.

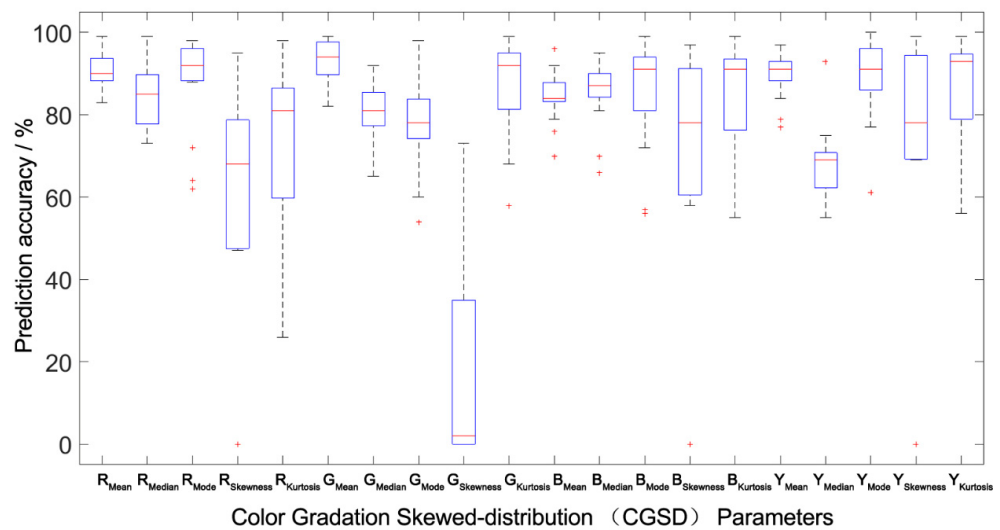


Figure 7. Prediction accuracy interval analysis of the population canopy color-meteorological response models of the outside-group. The *Boxplot* function of MATLAB was used to draw the accuracy

percentile distribution diagram of the population canopy CGSD parameters prediction model. The blue box in the figure represents the prediction accuracy of the model distributed between 25% and 75%. The shorter the box, the better the degree of data concentration. The red line in the box represents the median distribution of prediction accuracy, and the dotted line at both ends outside the box represents the endpoint value (maximum and minimum) of the prediction data distribution. The shorter the distance between the two endpoint values, the better the degree of data concentration. The red cross outside the box represents abnormal data. The fewer abnormal data, the better the degree of data distribution concentration.

3.4. Optimization of Canopy Color Skewness-Meteorological Models

Although the skewness of the red and green channels, and the gray-level image performed well, the between-group and outside-group prediction accuracy were generally lower than other CGSD parameters. The skewness was non-linear to microclimate factors [33]. Therefore, we fitted the polynomial Z1-Z4 that incorporates spatial bidirectional patterns for the RGB channels, and the gray-level image, by taking two accumulation factors, i.e., the accumulated temperature (x_1) and the accumulated photosynthetically active radiation (x_5) as the independent variables, which had the highest absolute value of the correlation coefficient.

$$Z1 = 0.3629 + 0.6382 \times 10^{-3} x_1 + 2.626 \times 10^{-3} x_5 + 5.312 \times 10^{-6} x_1^2 - 1.072 \times 10^{-5} x_1 x_5 \tag{4}$$

$$Z2 = 0.2242 + 0.5163 \times 10^{-3} x_1 + 3.11 \times 10^{-3} x_5 + 3.08 \times 10^{-6} x_1^2 - 7.463 \times 10^{-6} x_1 x_5 \tag{5}$$

$$Z3 = 0.3215 + 0.6477 \times 10^{-3} x_1 + 2.673 \times 10^{-3} x_5 + 3.93 \times 10^{-6} x_1^2 - 8.614 \times 10^{-6} x_1 x_5 \tag{6}$$

$$Z4 = 0.2786 + 0.5116 \times 10^{-3} x_1 + 3.114 \times 10^{-3} x_5 + 4.244 \times 10^{-6} x_1^2 - 9.285 \times 10^{-6} x_1 x_5 \tag{7}$$

After comparing the multiple stepwise regression and spatial bidirectional models using the skewness, the (R^2) of the spatial bidirectional models was higher than the multiple stepwise regression models with lower RMSE. This indicated that the nonlinear models had better fitting results, or the skewness of the population canopy image of BFH has a close relationship to the microclimate in the glass greenhouse (Table 5).

Table 5. Comparison of multiple stepwise regression models and spatial bidirectional models for the skewness.

Parameters	Model	R-Square	Adjusted R-Square	RMSE	Significant F
R _{Skewness}	Y4	0.803	0.791	0.142	0.000
	Z1 Equation (4)	0.884	0.874	0.111	0.000
G _{Skewness}	Y9	0.831	0.820	0.138	0.000
	Z2 Equation (5)	0.902	0.893	0.107	0.000
B _{Skewness}	Y14	0.791	0.782	0.145	0.000
	Z3 Equation (6)	0.900	0.891	0.102	0.000
Y _{Skewness}	Y19	0.784	0.775	0.156	0.000
	Z4 Equation (7)	0.894	0.884	0.111	0.000

The spatial bidirectional models for the skewness have 5.7 percentage points higher accuracy in prediction, and the number of outliers significantly decreased. Compared to the regression model, the average accuracy of the spatial bidirectional models was improved by 7.63, 5.75, and 6.25 percentage points in the modeling group, the between-group, and the outside-group, respectively. The RGB channels and gray-level image were all improved by 6.90, 10.87, 3.47, and 1.72 percentage points, respectively (Table 6).

Table 6. Comparison of the prediction accuracy of the multiple stepwise regression models and spatial bidirectional models for the skewness.

Parameters	Model	Prediction Sample Data	Modeling Group Eliminate Abnormal Data	Predictive Accuracy	Prediction Sample Data	Between-Group Eliminate Abnormal Data	Predictive Accuracy	Prediction Sample Data	Outside-Group Eliminate Abnormal Data	Predictive Accuracy	Average
R _{skewness}	Y4	51	0	80.98%	51	10	53.21%	15	3	70.30%	68.80%
	Z1	51	0	90.02%	51	1	60.56%	15	3	75.58%	77.76%
G _{skewness}	Y9	51	1	76.29%	51	9	52.40%	15	7	35.12%	63.73%
	Z2	51	0	88.31%	51	1	60.82%	15	3	73.71%	74.60%
B _{skewness}	Y14	51	1	82.21%	51	8	56.11%	15	3	82.39%	72.36%
	Z3	51	0	90.16%	51	1	61.27%	15	3	75.61%	75.83%
Y _{skewness}	Y19	51	2	80.43%	51	10	58.03%	15	3	84.64%	73.81%
	Z4	51	0	89.05%	51	1	60.10%	15	3	82.34%	75.53%

4. Discussion

The high quality and efficient production of greenhouse plants depend on the environmental regulation focusing on the plants’ growth in the facility. The changing physiological parameters result from the variation of temperature, radiation, and humidity rapidly and instantaneously [41–44]. Ineffective control of environmental factors will restrict the improvement of glass greenhouse yield and crop quality [45]. Therefore, coupling the relationship between the plant growth state indicated by color parameters and controlling the meteorological factors will help to promote the high quality and efficient production in facility plants, realize the precise control of the facility environment, and decrease the costs.

Digital color images’ information can reflect the growing state of plants [11], which provides a convenient way of plant growth monitoring. Research on conducting qualitative and quantitative descriptions of phenotypic traits for plant appearance by using digital imaging technology has increased in smart agriculture [6]. The RGB color model has been widely used to process digital color images to study chlorophyll content and its related plant nutritional status and stress response [24,46,47]. The RGB model and leaf color parameters can describe changes in tobacco leaf color depth and homogeneity [33]. Now, we found that images of the RGB channels and the gray-level images all showed a skewed distribution at the single leaf, plant, and population canopy images scale in BFH.

Environmental changes lead to changes in the color of plants’ leaves [21,26,48–50]. Our work indicated that temperature, humidity, ground temperature, soil temperature at 10 cm, and solar radiation in glass greenhouses were significantly correlated with multiple CGSD parameters of canopy images in BFH. Moreover, the accumulative value of temperature and solar radiation (AT, AGR, and APAR) had an extremely significant correlation with 20 CGSD parameters, with the correlation coefficients beyond 0.8. The mean, median, and mode parameters representing color depth have a positive relationship with the accumulative parameters, while the skewness and kurtosis parameters representing the color distribution showed a significantly negative correlation with the accumulative factors. The deep canopy color of BFH images has higher accumulative factors depending on the analysis of the peak changes of the cumulative distribution diagram of canopy color and provides a new approach to quantitative plant growing conditions.

The multi-dimensionality of CGSD parameters enables them to have a basis for building relationships with complex meteorological factors. Canopy color–meteorological responding models have high prediction accuracy after calculating the image mean, median, mode, and kurtosis parameters and skewness distribution using the spatial bidirectional models. The change of accumulative factors is generally linear, while skewness is calculated from a higher-order function. Although the skewness was significantly related to microclimate factors, it cannot be simply described and fitted by linear fitting [33]. Compared to the multiple stepwise regression models, the spatial bidirectional models had better fitness and higher accuracy.

The digital color image has been applied to automatic observation in agrometeorology [51,52], and is proposed as a new technical approach that can be combined with crop growth models [53], which agriculture meteorological services will automatically and intelligently apply in future services [54,55]. The relationship between the CGSD parameters of the population canopy and the environment meteorological factors makes it possible to

use the canopy color information to construct a plant growth model from digital images, which can provide new methods for quantitatively evaluating agricultural meteorological conditions, assessing agricultural meteorological disaster loss, predicting yield and quality, and supporting precise management of crop production.

5. Conclusions

Analyzing the canopy images' color histograms skewed distribution of BFH in the glasshouse, we found that 20 population canopy CGSD parameters were sensitive to the microclimate factors, especially the radiation and temperature accumulation factors. The canopy color–meteorological responding models showed that the CGSD parameters have a close relationship with microclimate factors, which expands the potential application of the RGB model in monitoring the variations of plant or leaf color. The CGSD parameters can describe the canopy color information comprehensively and accurately and are considered a new indicator for quantitative evaluation of plant growth conditions. These parameters help construct a plant growth condition model and provide a new method for agrometeorological assessment and prediction, and, ultimately, support the precise management of crop production.

Supplementary Materials: The following supporting information can be downloaded at: <https://www.mdpi.com/article/10.3390/atmos13060890/s1>, Table S1: Normal test of color distribution of a BFH population canopy.

Author Contributions: P.Z. and Z.C. are the Co-first authors. The work presented here was carried out in collaboration among all authors. P.Z., Z.C., F.W., C.L. and X.J. designed the study. P.Z. and R.W. conducted the research. Z.A., T.B., and X.X. processed the data, P.Z., Z.C., F.W. and X.X. analyzed the data result. P.Z. wrote the entire manuscript. C.L. edited the manuscript. All authors have read and agreed to the published version of the manuscript.

Funding: We are grateful for the grants from the “333 project” research project for the high-level talent of Jiangsu Province (Grant number BRA2019348) and the National Natural Science Foundation of China (Grant number 51309132).

Institutional Review Board Statement: Not applicable.

Informed Consent Statement: Not applicable.

Data Availability Statement: All datasets generated and analyzed for this study are included in the article/Supplementary Materials.

Conflicts of Interest: The authors declare that the research was conducted in the absence of any commercial or financial relationships that could be construed as a potential conflict of interest.

References

1. Zhou, H.L.; Zhou, G.S.; He, Q.J.; Zhou, L.; Ji, Y.H.; Zhou, M.Z. Environmental explanation of maize specific leaf area under varying water stress regimes. *Environ. Exp. Bot.* **2019**, *171*, 103932. [[CrossRef](#)]
2. Nawaz, R.; Abbasi, N.A.; Hafiz, I.A.; Khalid, A. Impact of climate variables on growth and development of Kinnow fruit (*Citrus nobilis* Lour × *Citrus deliciosa* Tenora) grown at different ecological zones under climate change scenario. *Sci. Hortic.* **2019**, *260*, 108868. [[CrossRef](#)]
3. Kempkes, F.; De Zwart, H.; Muñoz, P.; Montero, J.; Baptista, F.; Giuffrida, F.; Gilli, C.; Stępowaska, A.; Stanghellini, C. Heating and dehumidification in production greenhouses at northern latitudes: Energy use. *Acta Hortic.* **2017**, 445–452. [[CrossRef](#)]
4. Amani, M.; Foroushani, S.; Sultan, M.; Bahrami, M. Comprehensive review on dehumidification strategies for agricultural greenhouse applications. *Appl. Therm. Eng.* **2020**, *181*, 115979. [[CrossRef](#)]
5. Guo, Y.; Zhao, H.; Zhang, S.; Wang, Y.; Chow, D. Modeling and optimization of environment in agricultural greenhouses for improving cleaner and sustainable crop production. *J. Clean. Prod.* **2020**, *285*, 124843. [[CrossRef](#)]
6. Chen, D.; Neumann, K.; Friedel, S.; Kilian, B.; Chen, M.; Altmann, T.; Klukas, C. Dissecting the Phenotypic Components of Crop Plant Growth and Drought Responses Based on High-Throughput Image Analysis. *Plant Cell* **2014**, *26*, 4636–4655. [[CrossRef](#)]
7. He, J.Q.; Harrison, R.J.; Li, B. A novel 3D imaging system for strawberry phenotyping. *Plant Methods* **2017**, *13*, 1–8. [[CrossRef](#)]
8. Sancho-Adamson, M.; Trillas, M.I.; Bort, J.; Fernandez-Gallego, J.A.; Romanyà, J. Use of RGB Vegetation Indexes in Assessing Early Effects of Verticillium Wilt of Olive in Asymptomatic Plants in High and Low Fertility Scenarios. *Remote Sens.* **2019**, *11*, 607. [[CrossRef](#)]

9. Liu, Z.; Hu, H.; Yu, H.; Yang, X.; Yang, H.; Ruan, C.; Wang, Y.; Tang, J. Relationship between leaf physiologic traits and canopy color indices during the leaf expansion period in an oak forest. *Ecosphere* **2015**, *6*, art259. [[CrossRef](#)]
10. Grosskinsky, D.K.; Syaifullah, S.J.; Roitsch, T. Integration of multi-omics techniques and physiological phenotyping within a holistic phenomics approach to study senescence in model and crop plants. *J. Exp. Bot.* **2017**, *69*, 825–844. [[CrossRef](#)]
11. Vasseur, F.; Bresson, J.; Wang, G.; Schwab, R.; Weigel, D. Image-based methods for phenotyping growth dynamics and fitness components in *Arabidopsis thaliana*. *Plant Methods* **2018**, *14*, 1–11. [[CrossRef](#)]
12. Barker, J.; Zhang, N.Q.; Sharon, J.; Steeves, R.; Wang, X.; Wei, Y.; Poland, J. Development of a field-based high-throughput mobile phenotyping platform. *Comput. Electron. Agric.* **2016**, *122*, 74–85. [[CrossRef](#)]
13. Dey, A.K.; Sharma, M.; Meshram, M. An Analysis of Leaf Chlorophyll Measurement Method Using Chlorophyll Meter and Image Processing Technique. *Procedia Comput. Sci.* **2016**, *85*, 286–292. [[CrossRef](#)]
14. Yadav, S.P.; Ibaraki, Y.; Gupta, S.D. Estimation of the chlorophyll content of micropropagated potato plants using RGB based image analysis. *Plant Cell Tissue Organ. Cult. (PCTOC)* **2009**, *100*, 183–188. [[CrossRef](#)]
15. Adamsen, F.J.; Pinter, P.J.; Barnes, E.M.; Lamorte, R.L.; Wall, G.W.; Leavitt, S.W.; Kimball, B.A. Measuring Wheat Senescence with a Digital Camera. *Crop Sci.* **1999**, *39*, 719–724. [[CrossRef](#)]
16. Hu, H.; Liu, H.-Q.; Zhang, H.; Zhu, J.-H.; Yao, X.-G.; Zhang, X.-B.; Zheng, K.-F. Assessment of Chlorophyll Content Based on Image Color Analysis, Comparison with SPAD-502. In Proceedings of the 2nd International Conference on Information Engineering and Computer Science (ICIECS), Wuhan, China, 25–26 December 2010; pp. 476–478. [[CrossRef](#)]
17. Ali, M.M.; Al-Ani, A.; Eamus, D.; Tan, D.K.Y.A. New image processing based technique to determine chlorophyll in plants. *Am. Eurasian J. Agric. Environ. Sci.* **2012**, *12*, 1323–1328. [[CrossRef](#)]
18. Han, W.T.; Sun, Y.; Xu, T.F.; Chen, X.W.; Su, K.O. Detecting maize leaf water status by using digital RGB images. *Int. J. Agric. Biol. Eng.* **2014**, *7*, 45–53. [[CrossRef](#)]
19. Barbedo, J.G.A. Detection of nutrition deficiencies in plants using proximal images and machine learning: A review. *Comput. Electron. Agric.* **2019**, *162*, 482–492. [[CrossRef](#)]
20. Humplík, J.F.; Lazár, D.; Husičková, A.; Spíchal, L. Automated phenotyping of plant shoots using imaging methods for analysis of plant stress responses—A review. *Plant Methods* **2015**, *11*, 1–10. [[CrossRef](#)]
21. Humplík, J.F.; Lazár, D.; Fürst, T.; Husičková, A.; Hýbl, M.; Spíchal, L. Automated integrative high-throughput phenotyping of plant shoots: A case study of the cold-tolerance of pea (*Pisum sativum* L.). *Plant Methods* **2015**, *11*, 20. [[CrossRef](#)]
22. Bresson, J.; Bieker, S.; Riester, L.; Doll, J.; Zentgraf, U. A guideline for leaf senescence analyses: From quantification to physiological and molecular investigations. *J. Exp. Bot.* **2017**, *69*, 769–786. [[CrossRef](#)]
23. Li, L.; Zhang, Q.; Huang, D. A Review of Imaging Techniques for Plant Phenotyping. *Sensors* **2014**, *14*, 20078–20111. [[CrossRef](#)]
24. Neilson, E.H.; Edwards, A.M.; Blomstedt, C.K.; Berger, B.; Møller, B.L.; Gleadow, R.M. Utilization of a high-throughput shoot imaging system to examine the dynamic phenotypic responses of a C4 cereal crop plant to nitrogen and water deficiency over time. *J. Exp. Bot.* **2015**, *66*, 1817–1832. [[CrossRef](#)]
25. Bai, G.; Jenkins, S.; Yuan, W.; Graef, G.L.; Ge, Y. Field-Based Scoring of Soybean Iron Deficiency Chlorosis Using RGB Imaging and Statistical Learning. *Front. Plant Sci.* **2018**, *9*, 1002–1011. [[CrossRef](#)]
26. Gracia-Romero, A.; Kefauver, S.C.; Vergara-Díaz, O.; Zaman-Allah, M.; Prasanna, B.M.; Cairns, J.; Araus, J.L. Comparative Performance of Ground vs. Aerially Assessed RGB and Multispectral Indices for Early-Growth Evaluation of Maize Performance under Phosphorus Fertilization. *Front. Plant Sci.* **2017**, *8*, 2004. [[CrossRef](#)]
27. Tester, M.; Langridge, P. Breeding Technologies to Increase Crop Production in a Changing World. *Science* **2010**, *327*, 818–822. [[CrossRef](#)]
28. Bunce, J.A. Responses of stomatal conductance to light, humidity and temperature in winter wheat and barley grown at three concentrations of carbon dioxide in the field. *Global Change Biol* **2000**, *6*, 371–382. [[CrossRef](#)]
29. Min-Wha, J.; Mohammad, B.A.; Eun-Joo, H.; Kee-Yooup, P. Photosynthetic pigments, morphology and leaf gas exchange during ex vitro acclimatization of micropropagated CAM *Doritaenopsis* plantlets under relative humidity and air temperature. *Environ. Exp. Bot.* **2006**, *55*, 183–194. [[CrossRef](#)]
30. Urban, J.; Ingwers, M.W.; McGuire, M.A.; Teskey, R.O. Increase in leaf temperature opens stomata and decouples net photosynthesis from stomatal conductance in *Pinus taeda* and *Populus deltoides* x *nigra*. *J. Exp. Bot.* **2017**, *68*, 1757–1767. [[CrossRef](#)] [[PubMed](#)]
31. Wang, B.; Cai, W.; Li, J.; Wan, Y.; Li, Y.; Guo, C.; Wilkes, A.; You, S.; Qin, X.; Gao, Q.; et al. Leaf photosynthesis and stomatal conductance acclimate to elevated [CO₂] and temperature thus increasing dry matter productivity in a double rice cropping system. *Field Crop. Res.* **2020**, *248*, 107735. [[CrossRef](#)]
32. Gitelson, A.A.; Gritz, Y.; Merzlyak, M.N. Relationships between leaf chlorophyll content and spectral reflectance and algorithms for non-destructive chlorophyll assessment in higher plant leaves. *J. Plant Physiol.* **2003**, *160*, 271–282. [[CrossRef](#)]
33. Chen, Z.; Wang, F.; Zhang, P.; Ke, C.; Zhu, Y.; Cao, W.; Jiang, H. Skewed distribution of leaf color RGB model and application of skewed parameters in leaf color description model. *Plant Methods* **2020**, *16*, 23–28. [[CrossRef](#)]
34. Fukuoka, N.; Suzuki, T.; Minamide, K.; Hamada, T. Effect of Shading on Anthocyanin and Non-flavonoid Polyphenol Biosynthesis of *Gynura bicolor* Leaves in Midsummer. *HortScience* **2014**, *49*, 1148–1153. [[CrossRef](#)]
35. Ren, J.; Guo, S.S.; Xin, X.L.; Chen, L. Changes in volatile constituents and phenols from *Gynura bicolor* DC grown in elevated CO₂ and LED lighting. *Sci. Hortic.* **2014**, *175*, 243–250. [[CrossRef](#)]

36. Shimizu, Y.; Maeda, K.; Kato, M.; Shimomura, K. Methyl jasmonate induces anthocyanin accumulation in *Gynura bicolor* cultured roots. *Vitr. Cell Dev. Biol. Plant* **2010**, *46*, 460–465. [[CrossRef](#)]
37. Wu, C.-C.; Chang, Y.-P.; Wang, J.-J.; Liu, C.-H.; Wong, S.-L.; Jiang, C.-M.; Hsieh, S.-L. Dietary administration of *Gynura bicolor* (Roxb. Willd.) DC water extract enhances immune response and survival rate against *Vibrio alginolyticus* and white spot syndrome virus in white shrimp *Litopenaeus vannamei*. *Fish Shellfish Immunol.* **2014**, *42*, 25–33. [[CrossRef](#)]
38. Dobrescu, A.; Scorza, L.C.T.; Tsaftaris, S.A.; McCormick, A.J. A “Do-It-Yourself” phenotyping system: Measuring growth and morphology throughout the diel cycle in rosette shaped plants. *Plant Methods* **2017**, *13*, 1–12. [[CrossRef](#)]
39. Sun, Y.; Zhu, S.; Yang, X.; Weston, M.V.; Wang, K.; Shen, Z.; Xu, H.; Chen, L. Nitrogen diagnosis based on dynamic characteristics of rice leaf image. *PLoS ONE* **2018**, *13*, e0196298. [[CrossRef](#)]
40. Gai, J.Y. *Experimental Statistical Method*; China Agriculture Press: Beijing, China, 2000; pp. 193–208.
41. Hand, D. Effects of Atmospheric Humidity on Greenhouse Crops. *Acta Hort.* **1988**, *229*, 143–158. [[CrossRef](#)]
42. Shamshiri, R.R.; Jones, J.W.; Thorp, K.; Ahmad, D.; Man, H.C.; Taheri, S. Review of optimum temperature, humidity, and vapour pressure deficit for microclimate evaluation and control in greenhouse cultivation of tomato: A review. *Int. Agrophys.* **2018**, *32*, 287–302. [[CrossRef](#)]
43. Li, G.; Tang, L.; Zhang, X.; Dong, J.; Xiao, M. Factors affecting greenhouse microclimate and its regulating techniques: A review. *IOP Conf. Ser. Earth Environ. Sci.* **2018**, *167*, 012019. [[CrossRef](#)]
44. Singh, M.C.; Singh, J.P.; Pandey, S.K.; Cutting, N.G.; Sharma, P.; Shrivastav, V.; Sharma, P. A Review of Three Commonly Used Techniques of Controlling Greenhouse Microclimate. *Int. J. Curr. Microbiol. Appl. Sci.* **2018**, *7*, 3491–3505. [[CrossRef](#)]
45. Zhang, S.H.; Guo, Y.; Zhao, H.J.; Wang, Y.; Chow, D.; Fang, Y. Methodologies of control strategies for improving energy efficiency in agricultural greenhouses. *J. Clean. Prod.* **2020**, *274*, 122695. [[CrossRef](#)]
46. Zhu, J.-X.; Deng, J.-S.; Shi, Y.-Y.; Chen, Z.-L.; Han, N.; Wang, K. Diagnoses of rice nitrogen status based on characteristics of scanning leaf. *Spectrosc. Spect. Anal.* **2009**, *29*, 2171–2175. [[CrossRef](#)]
47. Chaerle, L.; Hagenbeek, D.; Vanrobaeys, X.; Van Der Straeten, D. Early detection of nutrient and biotic stress in *Phaseolus vulgaris*. *Int. J. Remote Sens.* **2007**, *28*, 3479–3492. [[CrossRef](#)]
48. Gous, P.W.; Meder, R.; Fox, G.P. Near Infrared Spectral Assessment of Stay-Green Barley Genotypes under Heat Stress. *J. Near Infrared Spectrosc.* **2015**, *23*, 145–153. [[CrossRef](#)]
49. Cai, J.; Okamoto, M.; Atieno, J.; Sutton, T.; Li, Y.; Miklavcic, S.J. Quantifying the Onset and Progression of Plant Senescence by Color Image Analysis for High Throughput Applications. *PLoS ONE* **2016**, *11*, e0157102. [[CrossRef](#)]
50. Schmalko, M.E.; Scipioni, P.G.; Ferreyra, D. Effect of Water Activity and Temperature in Color and Chlorophylls Changes in Yerba Mate Leaves. *Int. J. Food Prop.* **2005**, *8*, 313–322. [[CrossRef](#)]
51. Shibayama, M.; Sakamoto, T.; Takada, E.; Inoue, A.; Morita, K.; Takahashi, W.; Kimura, A. Estimating Paddy Rice Leaf Area Index with Fixed Point Continuous Observation of Near Infrared Reflectance Using a Calibrated Digital Camera. *Plant Prod. Sci.* **2011**, *14*, 30–46. [[CrossRef](#)]
52. Sritarapipat, T.; Rakwatin, P.; Kasetkasem, T. Automatic Rice Crop Height Measurement Using a Field Server and Digital Image Processing. *Sensors* **2014**, *14*, 900–926. [[CrossRef](#)]
53. Sun, Y.Y.; Shen, S.H. Research progress in application of crop growth models. *Chin. J. Agrometeorol.* **2019**, *40*, 444–459. [[CrossRef](#)]
54. Yu, Z.H.; Cao, Z.G.; Wu, X.; Bai, X.D.; Qin, Y.M.; Zhuo, W.; Xiao, Y.; Zhang, X.F.; Xue, H.X. Automatic image-based detection technology for two critical growth stages of maize: Emergence and three-leaf stage. *Agric. For. Meteorol.* **2013**, *174*, 65–84. [[CrossRef](#)]
55. Li, Y.; Cao, Z.; Lu, H.; Xiao, Y.; Zhu, Y.; Cremers, A.B. In-field cotton detection via region-based semantic image segmentation. *Comput. Electron. Agric.* **2016**, *127*, 475–486. [[CrossRef](#)]